Whey protein-loaded 3D-printed poly (lactic) acid scaffolds for wound dressing applications

To cite this article before publication: Hanne Meryem Kayadurmus *et al* 2024 *Biomed. Mater.* in press https://doi.org/10.1088/1748-605X/ad565d

Whey Protein-Loaded 3D-Printed Poly (lactic) Acid Scaffolds for Wound Dressing Applications

Hanne Meryem Kayadurmus[1,2], Azadeh Rezaei[3], Elif Ilhan[1], Sumeyye Cesur[1,2], Ali Sahin[4], Oguzhan Gunduz[1,2], Deepak M. Kalaskar[3], Nazmi Ekren[1,5]***

[1] Centre for Nanotechnology & Biomaterials Application and Research (NBUAM), Marmara University, Istanbul, Turkey

[2] Department of Metallurgical & Materials Engineering, Faculty of Technology, Marmara University, Istanbul, Turkey

[3] UCL Division of Surgery & Interventional Science, University College London, 9th Floor Royal Free Hospital, London NW3 2QG, UK

[4] Department of Biochemistry, School of Medicine / Genetic and Metabolic Diseases Research and Investigation Centre, Marmara University, Istanbul, Turkey

[5]Department of Electrical and Electronics Engineering, Faculty of Technology, Marmara University, Istanbul, Turkey

Corresponding authors

* nazmiekren@marmara.edu.tr , **d.kalaskar@ucl.ac.uk

ABSTRACT

Chronic skin wounds pose a global clinical challenge, necessitating effective treatment strategies. This study explores the potential of 3D printed Poly Lactic Acid (PLA) scaffolds, enhanced with Whey Protein Concentrate (WPC) at varying concentrations (25, 35, and 50% wt), for wound healing applications. PLA's biocompatibility, biodegradability, and thermal stability make it an ideal material for medical applications. The addition of WPC aims to mimic the skin's extracellular matrix and enhance the bioactivity of the PLA scaffolds. Fourier Transform Infrared Spectroscopy (FTIR) results confirmed the successful loading of WPC into the 3D printed PLA-based scaffolds. Scanning Electron Microscopy (SEM) images revealed no significant differences in pore size between PLA/WPC scaffolds and pure PLA scaffolds. Mechanical strength tests showed similar tensile strength between pure PLA and PLA with 50% WPC scaffolds. However, scaffolds with lower WPC concentrations displayed reduced tensile strength. Notably, all PLA/WPC scaffolds exhibited increased strain at break compared to pure PLA. Swelling capacity was highest in PLA with 25% WPC, approximately 130% higher than pure PLA. Scaffolds with higher WPC concentrations also showed increased swelling and degradation rates. Drug release was found to be prolonged with increasing WPC concentration. After seven days of incubation, cell viability significantly increased in PLA with 50% WPC scaffolds compared to pure PLA scaffolds. This innovative approach could pave the way for personalized wound care strategies, offering tailored treatments and targeted drug delivery. However, further studies are needed to optimize the properties of these scaffolds and validate their effectiveness in clinical settings.

Keywords: Tissue engineering scaffolds, 3D printing, Wound healing, Whey Protein Concentrate

1. INTRODUCTION

Repair of large and chronic skin wounds is amongst the most prevalent clinical challenges worldwide. The global occurrence of chronic wounds worldwide is approximated to range from 1.51 to 2.21 cases per 1000 individuals [1]. Major injuries from severe burns or medical conditions such as diabetes result in significant skin damage that hinders the natural process of skin regeneration [2]. Over the past few decades, skin grafting techniques have benefited many patients; however, there remain concerns regarding limited donor site[3] Such injuries may not only have a negative impact on a patient's quality of life but also present a tremendous financial burden to the healthcare systems [4].

Wounds are defined as disruption in the continuity of the epithelial lining of the skin or mucosa caused by chemical, mechanical, or thermal damage that results in loss of the defensive function of the tissue. The wound healing process repairs integrity of the damaged tissue and regenerates tissue that was lost [5]. Wound dressings have been utilized for many years for wound healing applications. The wound dressings play an important role in promoting wound healing and reducing scar formation and most importantly protecting the wound from further exogenous microorganisms, dehydration and pain [6,7]. In recent years interactive, advanced and smart dressing methods were studied by researchers. Smart dressings can perform multiple functions and also have the ability to treat with real-time monitoring with the help of sensors adjoined in the smart dressing [7]. Tamayol et al. developed the thermo-responsive nanofiber mesh to perform on-demand drug delivery and the drug was stimulated by biodegradable metallic heaters stacked on the nanofibers mesh [8].

Various polymeric scaffolds have been created to regenerate wound tissue. Three-dimensional (3D) printing, also known as additive manufacturing, represents a versatile and precise approach to wound care. 3D printing technology allows for the creation of multi-layered structures that supports cell adhesion and wound healing, encompassing its various layers [9].

Moreover, the adjustability of the 3D printed scaffold wound dressing's dimensional characteristics enables precise tailoring to individual patient needs. This flexibility extends to the easy incorporation of bioactive agents, allowing for targeted drug delivery [10].

There is an emerging interest in using 3D printed poly (lactic acid) (PLA) scaffolds for wound healing applications due to its in vivo potentiality [11,12]. PLA is considered as a gold standard for several 3D printing applications for medical use due to its excellent biocompatibility, biodegradability[13], thermal stability as well as versatility in fabrication [14,15]. PLA has also been reported to enhance the adhesion and proliferation in various cell types such as epidermal cells and fibroblasts [16].

Protein-based eco-friendly biomaterials such as dairy proteins are recently gathering attention as substitutes for commercial materials for biomedical applications [17]. To enhance the bioactivity of the 3D printed wound dressings and create extracellular matrix (ECM), protein-derived biomaterials can be added to the scaffold system [18–20]. Compared to other proteins such as ovalbumin, casein, beef, or soya, whey protein is considered to be the best quality protein available which comprises all the essential and non-essential amino acids and is an excellent source of glutamine and branched-chain amino acids, which are necessary for cell growth [21]. Whey Protein is the remaining liquid product after the casein separation from the milk protein which is one of the products of cheese-making and casein manufacturing in the dairy industry. Whey proteins contain 20% of the proteins in milk and include β-lactoglobulin (β-Lg; approximately 3.2 g/L), α-lactalbumin (α-La; approximately 1.2 g/L), bovine serum albumin (BSA; approximately 0.4 g/L), and immunoglobulins (approximately 0.7 g/L) [22]. Whey's bioactive peptides are known for their antioxidant, anti-inflammatory and antiviral properties [23,24]. Orally supplementing wounded diabetic rats using whey protein from raw camel milk has been shown to enhance normal inflammatory responses during wound healing compared to the nontreated animals [25]. Badr et. al. found that whey protein treatment

significantly decreased the elevated levels of pro-inflammatory cytokines (IL-1β, IL-6, and TNF-α) by restoring the levels of oxidative stress [26].

Whey protein studies in 3D printing applications are generally targeting food industry and bone tissue engineering. 3D fabricated wound dressing studies focusing on whey proteins combined with a synthetic polymer have not been performed for wound healing applications. This article will be first in literature that aims to fabricate 3D printed scaffolds using whey proteins, thus enhancing the wound healing process. In the context of the reports above, using the 3D printing technique, this study evaluated the fabrication of a novel composite wound dressing composed of PLA and WPC. To evaluate the potential of the suggested biomaterials, optimised scaffolds were further characterised for their morphological, chemical, and physical properties. The WPC release kinetics from 3D printed patches was also assessed. Finally, preliminary cellular compatibility studies were carried out using human fibroblast to determine whether our 3D printed patches are biocompatible for wound dressing applications. Our results suggest the possibility that PLA/WPC dressings may offer a rational therapeutic strategy for chronic wound healing.

2. Materials and methods

2.1. Materials

Biodegradable PLA (2003D) was supplied by NatureWorks LLC (Nebraska, USA). Cow milk WPC (Alfason; containing 93.74% (w/w) dry protein, 0.23% (w/w) fat, 0.061% (w/w) lactose, and 3.16% (w/w) ash) was kindly provided by Marmara University (Faculty of Technology). Dimethylformamide (DMF) and Dichloromethane (DCM) were obtained from Yasin Teknik (Istanbul, Türkiye). Human foreskin fibroblast cells (HFF) were purchased from American Type Culture Collection (ATCC). DAPI fluoresce stain, DMEM (Dulbecco's Modified Eagle Medium), Fetal Bovine Serum (FBS), penicillin/streptomycin, phosphate buffer saline (PBS) were purchased from Thermo Fisher Scientific (Massachusetts, USA).

2.2. Preparation of PLA/WPC 3D-printing solutions

The PLA stock solution was prepared by dissolving 1.7 g of PLA in a 10 ml co-solvent system of DMF and DCM (DMF: DCM=1:4, v/v) for 2 hours using a magnetic stirrer (WiseStir®, MSH-20A, Germany). WPC was diluted to 25%, 35%, and 50% in 10 ml of distilled deionised water using a magnetic stirrer. Each WPC solution was vortexed with PLA solution (WPC: PLA= 2:7 v/v) according to Table 1. In total, 4 scaffold groups were included in this study. All processes were done at room temperature.

Table 1. Composition of the 3D-printed scaffolds

3D-printed scaffolds	PLA content (wt %)	WPC content (wt %)
17PLA	17	0
17PLA/25WPC	17	25
17PLA/35WPC	17	35
17PLA/50WPC	17	50

2.3. Fabrication of the 3D printed scaffolds

SolidWorks simulation software (SolidWorks, MA, USA) was used to design the original 3D frame of the required scaffolds and the models were converted to G-codes in Slic3r software (Microsoft, CA, USA). The scaffolds were fabricated in an extrusion 3D printer (Hyrel 3D, SDS-5 Extruder, GA, USA) (Figure 1). The dimensions of the scaffolds were 20 mm x 20 mm x 0.5 mm with a total layer of 7 and an infill pattern of rectilinear. All scaffolds were designed with a height of layers of 0.024 mm and 96% infill density. PLA/WPC solutions were loaded into a 10 ml syringe directly connected to a needle with 0.2 mm diameter with a speed of 10mm/s and flow rate of 1ml/h. The printer head was controlled with an xyz speed of 25 mm/s. The printing was performed at room temperature and PLA/WPC solutions were solidified while printing. The solutions were printed on glass lams, and the print bed platform was maintained at room temperature to avoid PLA/WPC scaffold melting.

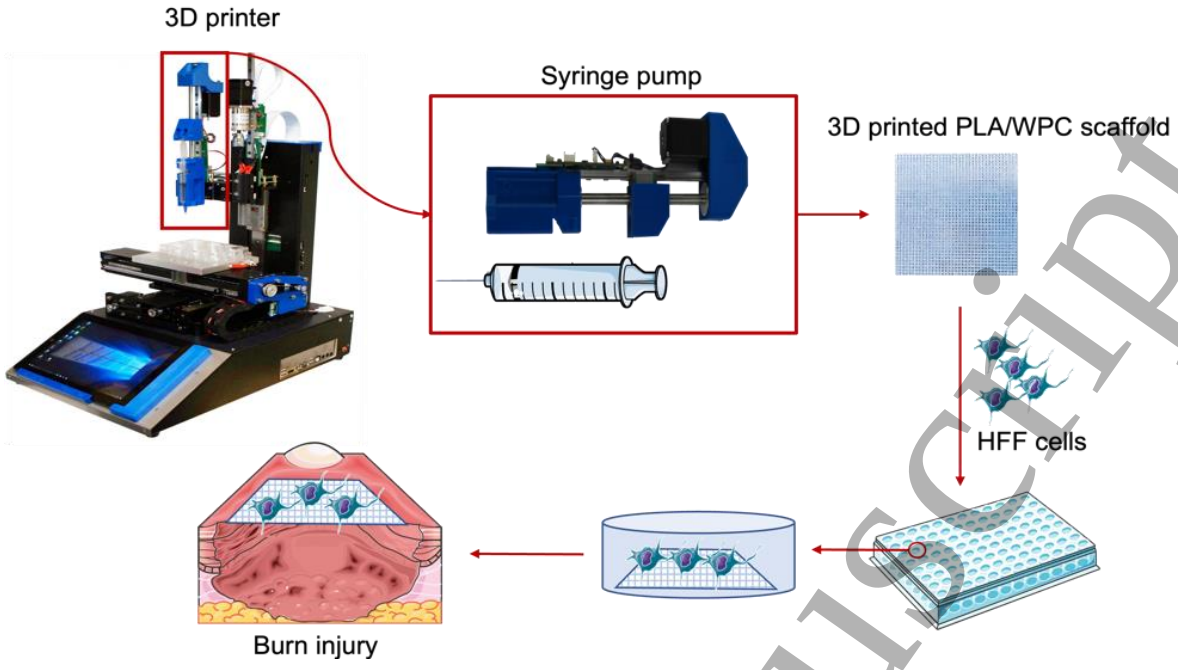

Figure 1. Schematic illustration of the 3D printer, 3D printed scaffolds, and wound dressing application (This figure was made with images available at Hyrel3D and Servier Medical Art)

2.4. Scaffold Characterisation

2.4.1. Fourier Transform Infrared (FTIR)

Fourier transform infrared spectrometer (Jasco, FT/IR 4700) equipped with Gladi attenuated total reflection (ATR) viewing plate (Diamond ATR crystal) and liquid-nitrogen cooled mercury cadmium telluride (MCT) detector was used to assess the chemical composition of the scaffolds. FTIR spectra were collected between and 4001 cm^{-1}, with a 4 cm^{-1} resolution and averaged over 32 scans. The spectra were processed and analysed using Spectra Manager (Jasco, Lecco, Italy) and KnowItAll Spectroscopy Library (Wiley Science Solutions, New Jersey, USA) software.

2.4.2. Scanning Electron Microscopy (SEM)

A ZEISS EVO MA 10 scanning electron microscope (SEM) was used to assess the surface topography and pore size of the scaffolds. The surface of the samples was gold coated for 120s

in a sputter coater (Quorum SC7620, Brighton, UK) to make them electroactive. Scaffolds were scanned with a voltage of 10 kV.

2.4.3. Pore Size Measurement

Using the SEM images obtained, the pore sizes of the scaffolds were calculated under an optical microscope (Olympus, AnalySIS, Tokyo, Japan). 50 random measurements were taken from each scaffold and the average pore size was calculated.

2.4.4. Tensile Properties of the Scaffolds

Tensile tests were performed using a SHIMADZU EZ-LX machine (Shimadzu Instruments, Kyoto, Japan) at a constant crosshead speed of 5mm/min and force of 0.1 N at room temperature. The upper and lower portions of each sample were located horizontally in the respective compartment of the device. The modulus, tensile strength, and elongation were calculated from the response obtained from the machine. The thickness of the scaffolds was also measured using a digital micrometre (Mitutoyo MTI Corporation, Tokyo, Japan). 4 group of scaffolds were analysed and 3 samples were selected as a subgroup.

2.4.5. Swelling and Degradation Rates of Scaffolds

To measure the swelling degree (SD) of the scaffold, briefly, the scaffolds were immersed in 1 ml phosphate-buffered saline solution (PBS; pH 7.4) for 0, 1, 2, 3, 4, 5, 6, and 7 days. The samples were kept on a thermal shaker (BIOSAN TS-100) at 37 °C throughout the experiment at 400 rpm. The PBS solution was regularly replaced at specified time points to maintain the biological environment activity. After the immersion time, samples were removed and slightly dried with filter paper before being weighed in the wet condition(W_w). Dry weight was also calculated before the immersion (W_o). The liquid absorption of each sample was calculated according to Eq. (1) to obtain swelling rates (S) [27];

$$S = \frac{(Ww - Wo)}{Wo}\ x100 \quad (1)$$

To assess the degradation degree of the scaffolds, samples were removed on days 0, 7,14, 21, and 30, washed with deionised water and then dried for 24 h at room temperature (W_t).

The degradation value (D) was calculated by using Eq.(2) [27];

$$D = \frac{(Wo - Wt)}{Wo} x100 \quad (2)$$

2.4.6. WPC encapsulation and release kinetic from scaffolds

To measure the release kinetics of WPC embedded in PLA/WPC scaffolds with various ratios (25%, 35%, and 50%) the scaffolds were cut into pieces of 5mg and suspended in 1 ml PBS (pH 7.4) and incubated at 37 °C for 24 h on shaker. At the scheduled time points (0, 0.25, 0.5, 1, 2, 3, 4, 6, 8, 12, and 24 h), PBS was removed and replaced with 1 mL of fresh PBS and UV spectroscopy (Shimadzu UV-3600) was used to measure the WPC release at 196 nm. A linear calibration curve was created using 5 different concentrations of WPC (2, 4, 6, 8, and 10 µg/mL) to calculate the release amount of WPC. The samples at all time points were run in triplicate. Encapsulation efficiency (%EE) represents the proportion of drug effectively loaded into the scaffolds. To assess the WPC content in the scaffolds, a standardized procedure was employed employing a UV-visible spectrophotometer (Shimadzu UV-3600, Kyoto, Japan). Initially, the scaffolds were fully dissolved in their respective solvent blends. Subsequently, the WPC quantities in the scaffolds were quantified using UV at 196 nm. WPC-loaded scaffolds, averaging 5 mg each, were dissolved in eppendorf with the addition of 10 mL of the solvent. Subsequently, 1 mL of each solution was taken and analyzed using a UV-visible spectrophotometer (Shimadzu UV-3600, Kyoto, Japan). All measurements were repeated three times for each of the three solutions. EE% was computed using the following formula:

$$\frac{\text{The mass of actual drug loaded in scaffolds}}{\text{Mass of drug used in scaffolds fabrication}} = EE\ \% \quad (3)$$

The drug release kinetics of the scaffolds was evaluated using different mathematical models such as Korsmeyer-Peppas (Eq.3), zero-order (Eq.4), first-order (Eq.5), Higuchi (Eq.6), and Hixson-Crowell (Eq.7), using the below equations:

$$Q = Kt^n \quad (4)$$

$$Q = K_0 t \quad (5)$$

$$\ln (1-Q) = -K_1 t \quad (6)$$

$$Q = K_h t^{1/2} \quad (7)$$

$$Q^{1/3} = K_{hc} t \quad (8)$$

In these equations, Q is the fractional amount of drug release at time t; K, K0, K1, Kh, and Khc are the kinetic constants for Korsmeyer-Peppas, zero-order, first-order, Higuchi, and Hixson-Crowell models, respectively. N is the diffusion exponent, which is indicative of the drug release mechanism. All measurements were repeated 3 times.

2.5. Cell culture assays

2.5.1 Cell seeding

Human foreskin fibroblast (HFF) cells were cultured in DMEM supplemented with 10% FBS and 100 U/ml penicillin and 0.1 mg/ml of streptomycin and kept at 37° C and 5% CO_2 incubator (SANYO, Osaka, Japan) until reaching 70% confluency. The scaffolds (17PLA, 17PLA/25 WPC, 17PLA/35 WPC, 17PLA/50 WPC) were cut to be circular in 6mm radius and plated in 96 well plates and sterilised under an ultraviolet (UV) lamp overnight. To allow protein adsorption and improve cell adhesion, the scaffolds were pre-incubated in DMEM for 1h at 37° C before cell seeding. After incubation, the medium was discarded, and the cells were seeded at a density of 5 x 10^4 cells per well and were incubated for 1, 4 and 7 days. Wells without scaffolds were used as controls.

2.5.2 Cell viability assay

Cell viability was assessed using the Thiazolyl Blue tetrazolium bromide, MTT assay (Glentham Life Sciences). On days 1, 4, and 7, supernatant was removed and scaffolds were washed with PBS. 20 μL of MTT reaction solution (5 mg/mL) in DMEM was added into each well and cells were kept in an incubator (37°C, 5%CO_2) for 3 h. Following the incubation period, a purple medium containing formazan crystals was acquired as a result of MTT reduction by viable cells. The supernatant on the scaffolds was discarded and to solubilise the formazan crystals, 100 μL of DMSO-ethanol (1:1 v/v) solution was added to each well and the plates were shaken gently for 10 seconds. The absorbance was measured at 560 nm (against 690 nm reference) in a microplate reader (Perkin Elmer Enspire, Singapore).

2.5.3 Cell attachment studies

2.5.3.1 DAPI staining

Fluorescence microscopy analysis was used to investigate the cell attachment on/into 3D printed scaffolds. After culturing the cells on the scaffolds for 1, 4, and 7 days, the supernatant was washed with PBS and the attached cells on the scaffolds were fixed in 4% paraformaldehyde (PFA, SantaCruz) for 30 min. The scaffolds were then washed with PBS and mounted using 1 μg/ml DAPI (ThermoFisher) nuclear stain for 20 min in the dark room. An inverted fluorescence microscope (Leica, Hamburg, Germany) was used to image the cells immediately. All incubations were conducted at room temperature.

2.5.3.2 SEM imaging

The cell attachment was also assessed using SEM after 1, 4, and 7 days. Briefly, the supernatant was discarded, and the scaffolds were washed with PBS. The fixation of the cells was done with 4% PFA for 30 minutes. The scaffolds were then dehydrated in an ethanol-graded series

(25, 50, 70 90, and 100%) for 5 min each and air-dried at room temperature. The scaffolds were observed by SEM (EVO LS 10, ZEISS Istanbul, Turkey) after gold coating (Quorum SC7620, Brighton, UK).

2.6 Statistical analysis

The results were expressed as mean ± standard deviation (SD). All analyses were performed using SPSS 17.0 software (SPSS Inc, Chicago, IL, USA) unless otherwise stated. Post-hoc one-way ANOVA with a Tukey-Kramer pair-wise comparison were used to analyse the differences between the control and experimental groups. The differences were considered statistically significant at $p<0.05$.

3. RESULTS

3.1. Compositional Analysis of PLA/WPC scaffolds

The scaffolds (17PLA, 17PLA/25 WPC, 17PLA/35 WPC, 17PLA/50 WPC) were characterised by FTIR spectra as shown in Fig.2. Pure PLA (Fig.2A), main absorption bands showed C=O vibration peak at 1749 cm^{-1}, CH_3 asymmetrical shear at 1453 cm^{-1}, CH_3 and C-H bending vibrations 1381 and 1356 cm^{-1}, C–O–C stretching at 1080 cm^{-1}, C–CH_3 stretching at 1042 cm^{-1} and C–COO stretching peak at 865 cm^{-1} [28,29]. Pure WPC (Fig.2B) revealed a peak at ~3272 cm^{-1} corresponding to C–H stretching of hydrogen bonding and peaks at ~2961 cm^{-1} and 2927 cm^{-1} corresponding to -CH_2 groups [30,31]. Fig.2C, 2D, 2E exhibits the FTIR spectra of 17PLA/25WPC, 17PLA/35WPC, 17PLA/50WPC scaffolds, respectively. In WPC-loaded scaffolds, minor shifts in peak positions were detected compared to the main peaks of pure PLA and pure WPC. Although the peaks of PLA are generally dominant in the scaffolds, a C-H band at 3272 cm^{-1} belonging to WPC is observed in every scaffold containing WPC which confirms successful loading of WPC into 3D printed scaffolds. In addition, the peaks of the amide groups of WPC at 1627 cm^{-1} and 1525 cm^{-1} increased their dominance depending on the increasing WPC concentration.

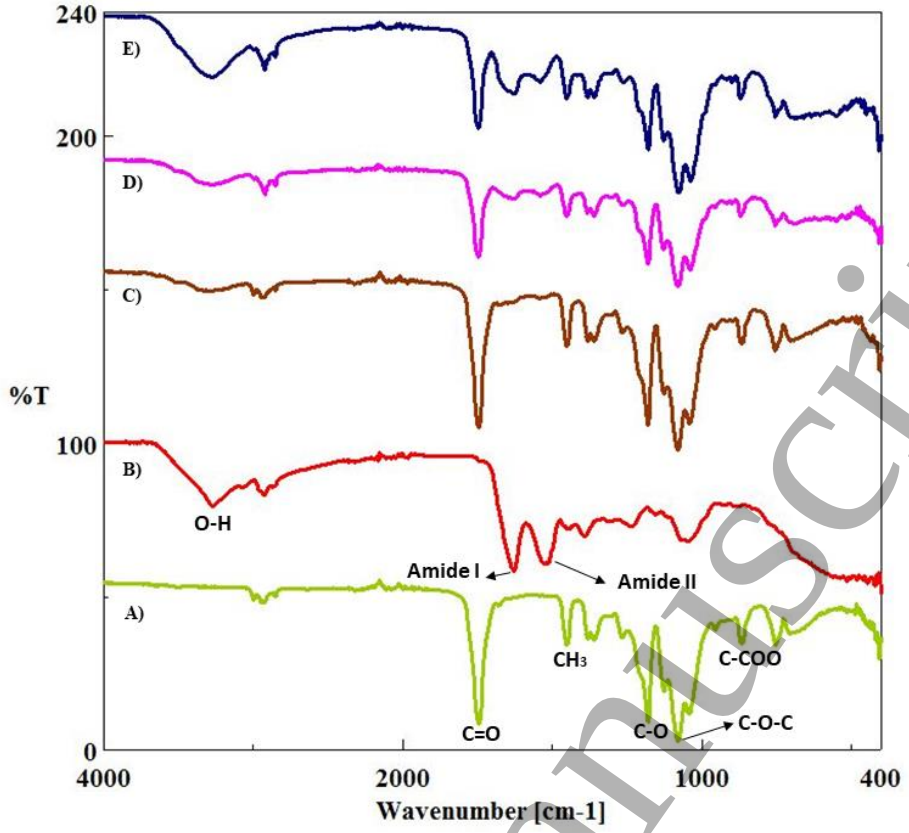

Figure 2. FTIR spectrums of the pure PLA (A), pure WPC (B) and 17PLA/25WPC (C), 17PLA/35WPC (D), and 17PLA/50WPC (E) scaffolds.

3.2 Morphological Observations

SEM images (Fig.3) showed that both pure PLA and WPC and composite scaffolds (17PLA/25WPC, 17PLA/35WPC, 17PLA/50WPC) contained open, evenly distributed and easily distinguishable (from each other) pores. Pure PLA (Fig.3A) showed an average pore size of 216.02±20µm. No statistically significant differences were found between pure PLA and 17PLA/25WPC (236.69±33µm), 17PLA/35WPC (189.33±42µm), and 17PLA/50WPC (217.11±28µm) as shown in Fig3.B,C and D, respectively.

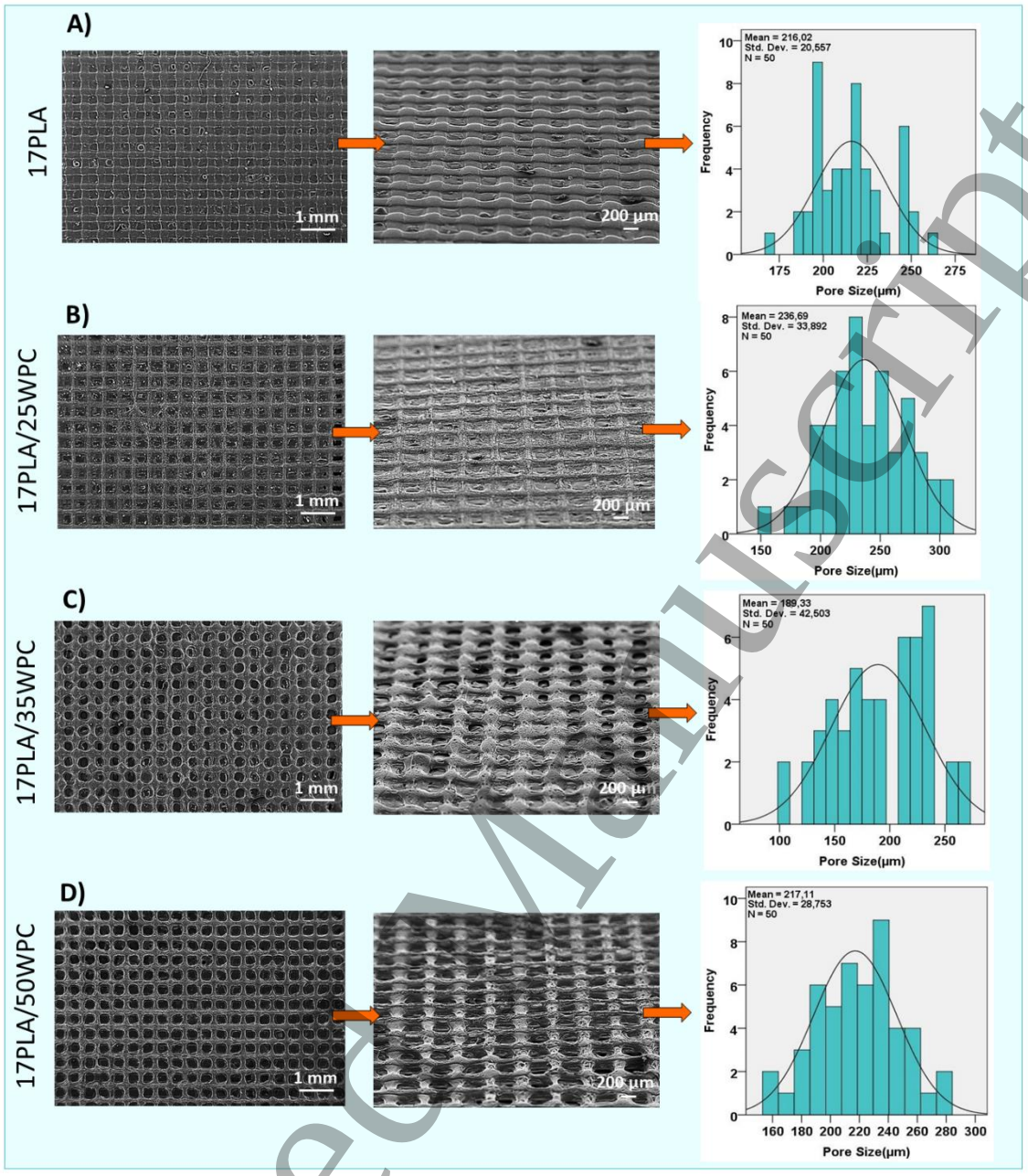

Figure 3. SEM images and pore size analysis of pure PLA (A), 17PLA/25WPC (B), 17PLA/35WPC (C), and 17PLA/50WPC (D) scaffolds.

3.3 Mechanical Characterization

Table 2 shows the data corresponding to the tensile strength and strain at the break for the PLA scaffolds both with and without WPC. The incorporation of 50% WPC into the PLA scaffold (17PLA/50WPC) exhibited similar tensile strength to the pure PLA scaffold, whereas lower

WPC concentrations 25% and 35%) displayed significantly reduced ($P<0.05$) tensile strength compared to the pure PLA. Moreover, pure PLA scaffolds showed the lowest strain at the break, while addition of WPC to the PLA scaffolds at all concentrations resulted in a significant increase in strain at break. Notably, the less the WPC content, the greater the strain at break.

Table 2: Tensile test measurements of scaffolds (mean ± SD) **P≤0.0.1, ****P≤0.0001 (n=3)

Scaffolds	Tensile Strength (MPa)	Strain at Break (%)
17PLA	43.13 ± 4.7	21.42 ± 3.8
17PLA/25WPC	11.24 ± 2.8****	55.47 ± 2.4****
17PLA/35WPC	30.28 ± 7.6**	41.45 ± 8.2****
17PLA/50WPC	38.18 ± 2.3	35.85 ± 2.9****

3.4 Swelling capacity and degradation behavior

As illustrated in Fig 4.A, after 7 days, the highest swelling rate was observed in the PLA scaffold loaded with 25% WPC (17PLA/25WPC), which was approximately 130% higher than that of the pure PLA scaffold. The incorporation of higher amounts of WPC (35% and 50%) also resulted in an increased swelling rate, which was about 60% higher compared to the pure PLA scaffold. As anticipated, the PLA scaffold incorporated with 25% WPC demonstrated the highest degradation rate of approximately 20% after a period of 30 days (Fig.4B). Scaffolds with higher WPC concentrations (35% and 50%) also exhibited an increased degradation rate compared to the pure PLA scaffold. Notably, up to day 14, the degradation rates across different WPC concentrations did not show significant differences. However, post day 14, the PLA scaffolds with 25% WPC exhibited a higher rate of degradation. In accordance with obtained results, it was observed that the degradation process was directly proportional to the swelling across all four different scaffold types.

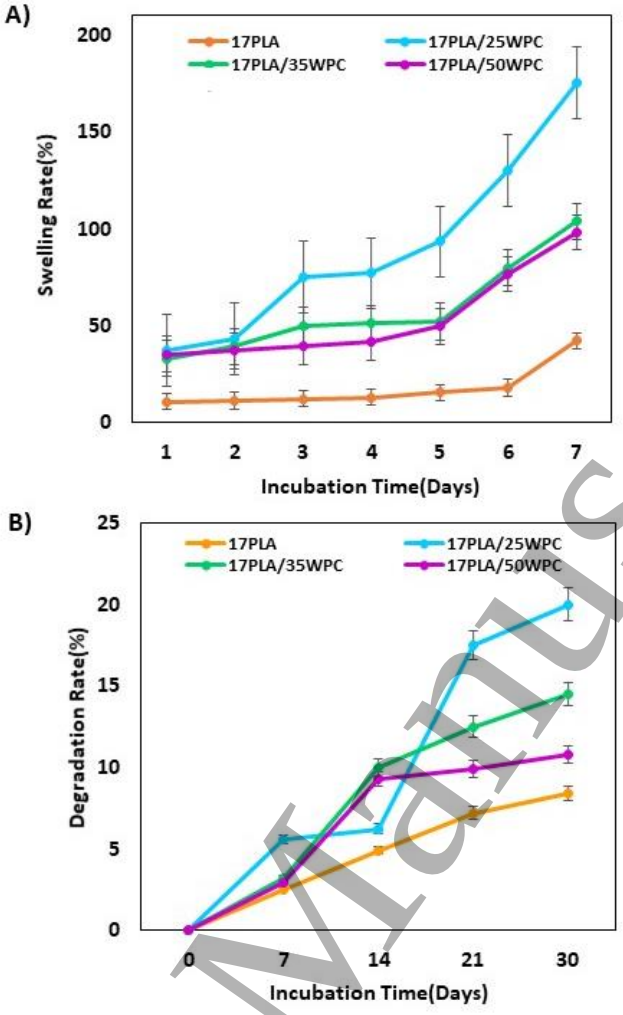

Figure 4. Swelling (A) and Degradation behaviours (B) of 17PLA, 17PLA/25WPC, 17PLA/35WPC, and 17PLA/50WPC scaffolds in PBS 7.4 at 37 °C. (n=3)

3.5 In vitro drug release and kinetics

To calculate the release of WPC from the 3D printed scaffold into PBS (pH 7.4), a linear standard calibration curve was plotted from the UV spectra at 196nm of the WPC between concentrations of 2 and 10µg/mL (Fig.5A and B). As shown in Fig.5C, all WPC-loaded scaffolds exhibited an initial burst drug release within the first 12 hours, which can be attributed to the excellent solubility of whey protein in PBS across a wide range of pH (from pH 2 to 9). However, it is important to note that the release rates varied amongst scaffolds with different

concentrations of WPC. After 24-hour period, the release rates of 17 PLA/25 WPC, 17 PLA/35WPC, and 17PLA/50 WPC scaffolds were recorded as %94.2, %97.6, and %83.7, respectively. The 17PLA/25WPC scaffold halted drug release at the end of day 2, while the 17PLA/35WPC scaffold reached complete (100%) drug release by day 5 and the 17PLA/50WPC scaffold reached complete drug release by day 7. These results indicate that although all three scaffolds exhibited burst drug release at the end of first day, drug release was prolonged with increasing WPC concentration. Apart from this, the encapsulation efficiency (EE) of WPC into the scaffolds was determined. Encapsulation efficiency in 17PLA/25WPC, 17PLA/35WPC and 17PLA/50WPC were determined as 82.91%, 75.70%, and 69.73% respectively.

The release kinetics of the produced scaffolds loaded with WPC at different concentrations were also investigated with Korsmeyer-Peppas, Zero-Order, First-Order, Higuchi, Hixon-Crowell models (Supplementary Data Fig.1). The kinetic rate constants (k) and the correlation coefficients (R^2) and for Korsmeyer-Peppas model the release exponent (n) obtained for all nanofiber scaffolds are given in Table 3. The drug release kinetics in the scaffolds were best described by the Korsmeyer-Peppas kinetic model, as indicated by the highest R^2 correlation coefficient. All three scaffolds exhibited drug release following the Korsmeyer-Peppas model, with "n" values indicative of Fickian diffusion model ($n<0.45$) (Table 3 and 4) [32].

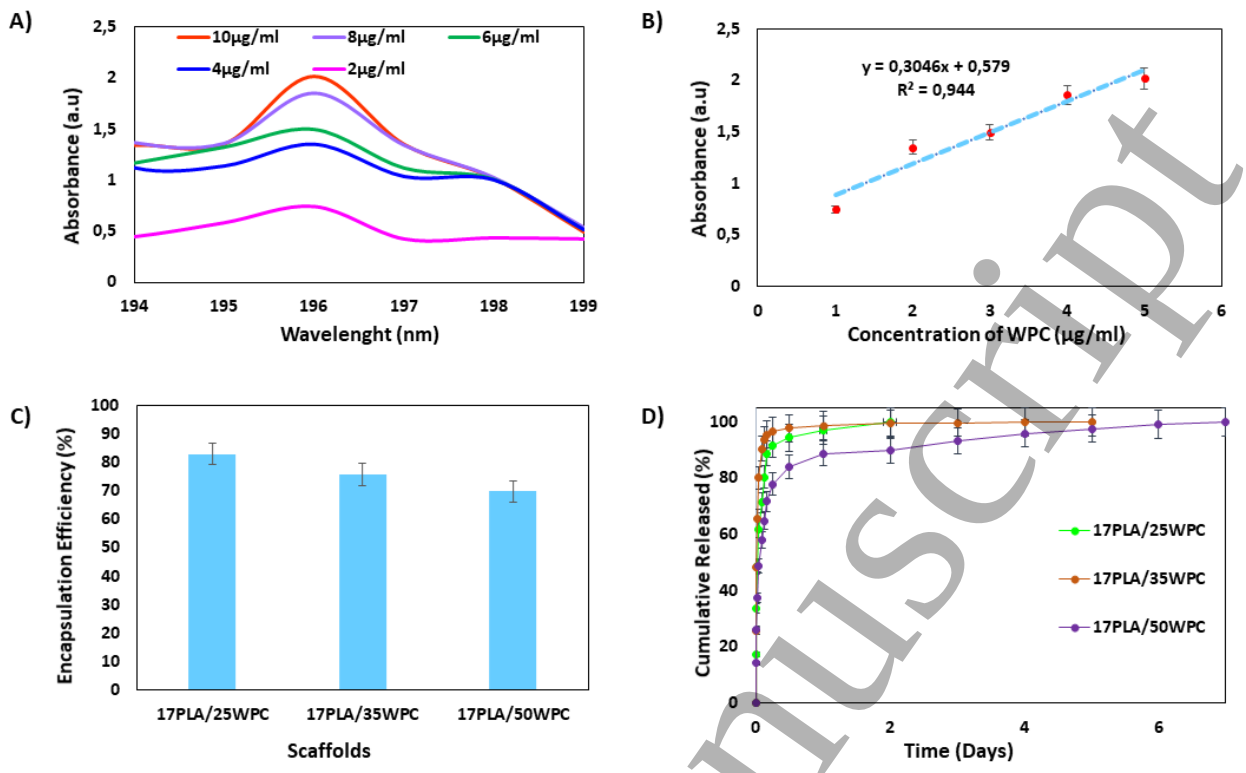

Figure 5. In vitro drug release profiles of scaffolds. Absorption spectra of WPC at different concentrations (A), WPC calibration curve (B), Encapsulation Efficiency (%) (C), and Cumulative WPC release profiles from different scaffolds (C). (n=3)

Table 3. Values of mathematical drug release models for the studies scaffolds.

	Korsmeyer-Peppas		Zero-Order		First-Order		Higuchi		Hixson-Crowell	
Sample	R^2	**n**	R^2	K_0	R^2	K_1	R^2	K_h	R^2	K_{hc}
17PLA/25WPC	0.9326	0.106	0.3342	1.3608	0.7725	-0.038	0.6045	12.624	0.7343	0.081
17PLA/35WPC	0.8814	0.042	0.2033	0.3558	0.5909	-0.037	0.3643	5.1033	0.5368	0.026
17PLA/50WPC	0.9112	0.121	0.4749	0.3855	0.8889	-0.011	0.6663	5.7452	0.8218	0.02

Table 4. Korsmeyer-Peppas Mode Drug Release mechanism

Exponent (n)	Drug release-mechanism

$0.45 \leq n$	Fickian diffusion mechanism
$0.45 < n < 0.89$	Non-Fickian diffusion
$n = 0.89$	Zero order release
$n > 0.89$	Super case II transport

3.6. Cell Adhesion

Cell adhesion was investigated from three distinct perspectives. Cell viability was determined via the MTT assay (Fig.6), and cell morphology was characterised using SEM (Fig.7A) and immunofluorescence staining (Fig.7B). On day 1, both 17PLA/25WPC, and 17PLA/50WPC scaffolds demonstrated a significant enhancement in cell viability in comparison to the 2D control group. However, following a 3-day incubation period, only the cells in pure PLA scaffolds demonstrated an increase in cell viability. In contrast, the WPC scaffolds, irrespective of their concentration, did not exhibit any significant changed. Upon extending the incubation period to 7 days, a substantial increase was observed in both pure PLA scaffold and the 17PLA/50WPC scaffold. However, the 17PLA/35WPC scaffold did not exhibit any significant changes, while the 17PLA/25WPC scaffold experienced a notable decrease in cell viability.

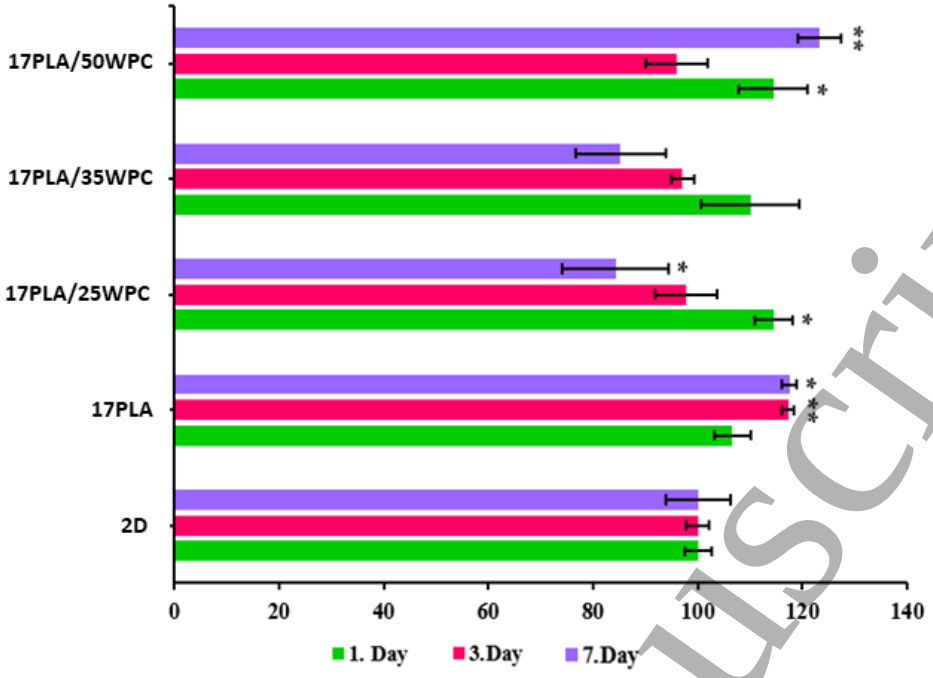

Figure 6. Cell viability analysis of 17PLA, 17PLA/25WPC, 17PLA/35WPC, and 17PLA/50WPC scaffolds. (n=3) (*p ≤ 0,05, **p ≤0,01).

On day 7, cells had spread and formed extensions (Fig.7A). Fig.7B also revealed high viable cell densities across all scaffolds, corroborated by MTT results indicating over 80% viability in each scaffold.

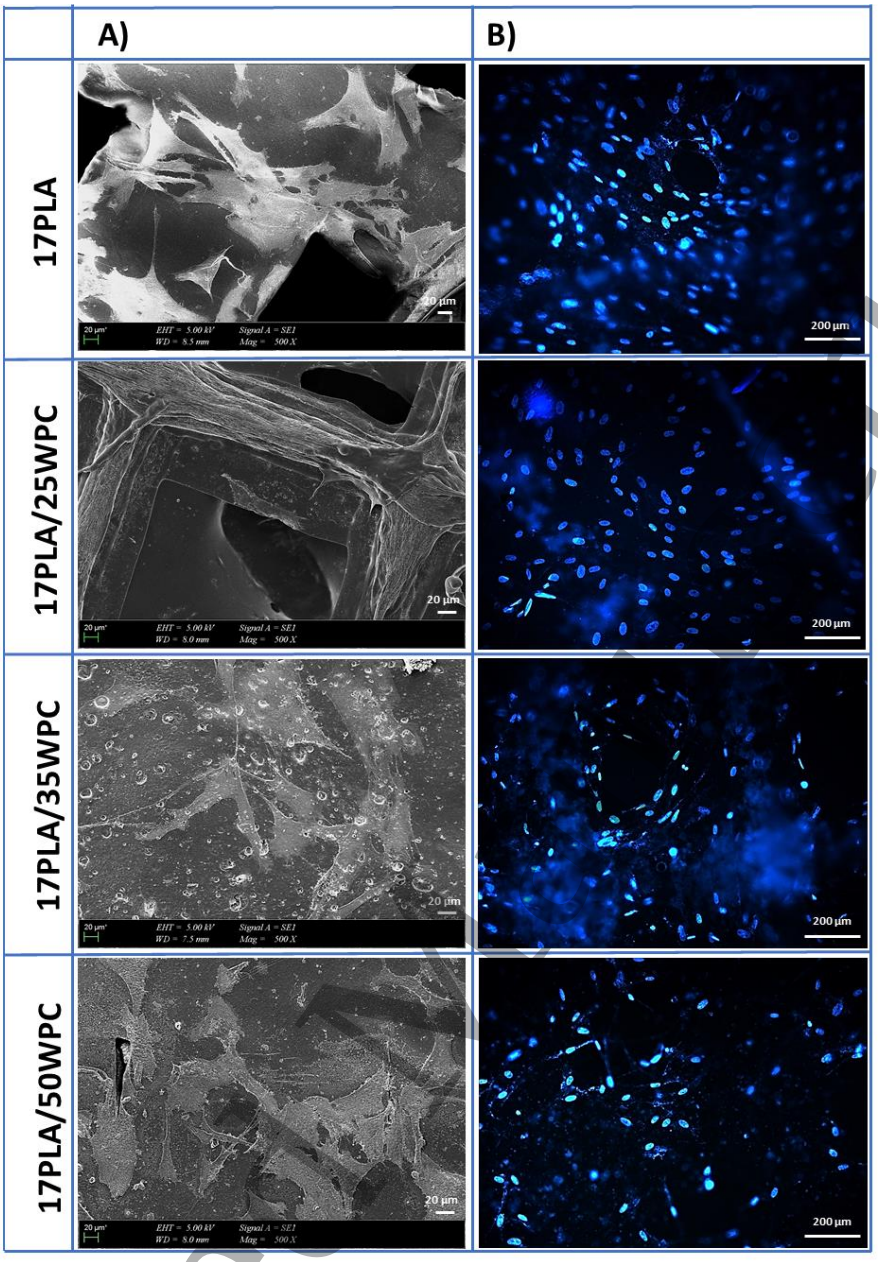

Figure 7. SEM images of HFF-1 cells on 17PLA, 17PLA/25WPC, 17PLA/35WPC, and 17PLA/50WPC scaffolds (A) and fluorescence images of attached cells on 17PLA, 17PLA/25WPC, 17PLA/35WPC, and 17PLA/50WPC scaffolds (B) after 7 days of incubation.

4. DISCUSSION

The process of wound healing is a complex physiological phenomenon that necessitates an increased intake of proteins and amino acids. Medical professionals often prescribe whey protein to patients with burns or post-surgical wounds to expedite the healing process [33,34]. This is attributed to the comprehensive amino acid profile of whey protein, which encompasses both essential and non-essential amino acids, including arginine, glycine, leucine, isoleucine, and valine. These specific amino acids play a pivotal role in the regeneration of bones, skin, and muscle tissues [35]. Furthermore, dietary supplementation with whey protein has been observed to enhance the standard inflammatory responses during wound healing in diabetic mice by restoring the balance of oxidative stress and inflammatory cytokines [25]. Compared to other protein sources such as ovalbumin, casein, beef meat, or soy, whey protein is deemed superior in quality. It serves as an excellent source of glutamine and branched-chain amino acids, both of which are integral for cellular growth. Consequently, the high concentration of these crucial amino acids in whey significantly contributes to wound healing [35].

In this study, we have fabricated and characterised scaffolds composed of poly lactic acid (PLA) incorporated with whey protein concentrate (WPC) for the first time to improve biocompatibility of PLA. FTIR results showed that although the peaks of PLA are generally dominant in the scaffolds, a C-H band belonging to WPC is observed in every scaffold containing WPC. This confirms successful loading of WPC into 3D printed scaffolds.

Our scaffolds exhibited an average pore size of less than 300 μm, adhering to the theoretical value of 100-300 μm for tissue engineering constructs. The minimum requirement for pore size is ~100 μm due to cell size, migration requirements and transport. However, pore sizes >300 μm are recommended, due to enhanced formation of capillaries [36]. In the CAD program, the scaffolding was designed to be 20 mm x 20 mm x 0.5 mm (X, Y, Z) and 96%

infill density. The dimensions of the produced scaffolds were measured as approximately 20 mm x 20 mm x 0.35 mm (X, Y, Z). Although the X and Y dimensions were obtained in almost the same proportions, a slight reduction in the Z dimension was observed after production. Particularly, the decrease in the Z dimension can be explained by the spread of the liquid polymer from the needle tip onto the glass coverslip.

Numerous studies have indicated that under SEM, the surface morphologies of PLA microspheres are typically smooth and devoid of pores [37,38]. In line with these findings, the SEM images obtained in this study revealed that pure PLA scaffolds also exhibited a smooth surface. However, upon incorporation of WPC, the scaffolds displayed micropore structures and rough surfaces. The roughness of PLA/WPC would aid in cell attachment, which aligns with our MTT results where the addition of 50%WPC showed more metabolic activity in the HFF cells compared to pure PLA. The latter has a smooth surface and curved pores, causing cells to flow downwards due to the potential energy of gravity, resulting in poorer cell attachment [39].

The decrease in swelling potential with increasing WPC concentration (17PLA/35WPC and 17PLA/50WPC) can be explained by Florey's theory. At a higher concentration, the density of the protein network is greater, so the swelling rate should decrease with increasing protein concentration [40]. The addition of WPC to PLA increased the desired swelling and degradation properties of an ideal dressing and exhibited controlled release behaviors for up to 7 days. In addition, increasing the amount of protein in the medium may cause agglomeration. This may prevent the formation of a homogeneous mixture and reduce encapsulation efficiency. The decrease in the encapsulation rate as the amou nt of WPC increases can be attributed to this reason [41]. The drug kinetic results showed that scaffolds with different WPC concentrations (25%, 35%, and 50%) followed the Korsmeyer-Peppas kinetic pattern and WPC was released from the scaffolds via the Fickian diffusion mechanism. The percentage of strain

at break for the PLA scaffold demonstrated an increase with the incorporation of all concentrations of WPC, indicating good compatibility between PLA and WPC that didn't generate any discontinuities in the PLA matrix. This enhancement can be attributed to the introduction of the helical structure inherent to proteins, which are known to exhibit viscoelastic behaviour upon the application of strain [42,43].

Consequently, this leads to an improvement in the elongation at break for the polymer materials. Interestingly, PLA scaffolds with the lowest amount of WPC (17PLA/25WPC) showed the highest value for strain at break percentage which surprisingly didn't reduced the swelling ratio at this concentration. This concentration (17PLA/25WPC) also showed the highest degradation rate. Results also indicate that although all three scaffolds exhibited burst drug release at the end of first day, drug release was prolonged with increasing WPC concentration and 17PLA/50WPC had the most prolonged release probably due to less wt% of PLA and quicker degradation process of PLA [44].

Based on these findings, the PLA/WPC scaffold developed in this study demonstrates promising potential as a wound dressing for patients with specific needs. The scaffold's ability to tailor the release of whey protein, a known enhancer of wound healing, is particularly beneficial. Therefore, this PLA/WPC scaffold represents a significant advancement in the field of wound care, offering a customisable solution that can be tailored to meet individual patient needs.

5. CONCLUSION

In conclusion, this study successfully developed scaffolds using 3D-printing technology with PLA and WPC, achieving average pore sizes between 100-300 μm, making them suitable for wound dressing applications. The successful incorporation of WPC into the 3D printed scaffolds, as confirmed by FTIR results, along with the observed increase in biocompatibility

and cellular metabolic activity, further supports this potential. The scaffold's enhanced swelling and degradation properties, controlled release behaviors, and improved strain of break with the addition of WPC all contribute to its suitability as an ideal dressing. Moreover, the scaffold's ability to follow the Korsmeyer-Peppas kinetic pattern and release WPC via the Fickian diffusion mechanism allows for a controlled and sustained delivery of proteins necessary for wound healing. Based on these findings, it can be recommended that PLA/WPC scaffolds obtained by the 3D printing method be considered as an alternative solution for potential wound treatment applications.

Referances

[1] UfkayKarabay MehtapYüksel Eğrilmez, HasanHavıtçıoğlu R B 2019 Dermal Doku Mühendisliği Uygulaması için 3B Baskılı Doku İskelesi: In vitro Fibroblast Proliferasyonu *Journal* **1** 51–6

[2] Martinengo L, Olsson M, Bajpai R, Soljak M, Upton Z, Schmidtchen A, Car J and Järbrink K 2019 Prevalence of chronic wounds in the general population: systematic review and meta-analysis of observational studies *Ann Epidemiol* **29** 8–15

[3] Dolp R, Rehou S, Pinto R, Trister R and Jeschke M G 2019 The effect of diabetes on burn patients: a retrospective cohort study. *Crit Care* **23** 28

[4] Rettinger C L, Fletcher J L, Carlsson A H and Chan R K 2017 Accelerated epithelialization and improved wound healing metrics in porcine full-thickness wounds transplanted with full-thickness skin micrografts. *Wound Repair Regen* **25** 816–27

[5] Kus K J B and Ruiz E S 2020 Wound Dressings – A Practical Review *Curr Dermatol Rep* **9**

[6] Varaprasad K, Jayaramudu T, Kanikireddy V, Toro C and Sadiku E R 2020 Alginate-based composite materials for wound dressing application:A mini review *Carbohydr Polym* **236**

[7] Ambekar R S and Kandasubramanian B 2019 Advancements in nanofibers for wound dressing: A review *Eur Polym J* **117**

[8] Tamayol A, Hassani Najafabadi A, Mostafalu P, Yetisen A K, Commotto M, Aldhahri M, Abdel-Wahab M S, Najafabadi Z I, Latifi S, Akbari M, Annabi N, Yun S H, Memic A, Dokmeci M R and Khademhosseini A 2017 Biodegradable elastic nanofibrous platforms with integrated flexible heaters for on-demand drug delivery *Sci Rep* **7**

[9] Iliyasu Datti Gwarzo Siti Pauliena Mohd Bohari R A W and Zia A 2022 Recent advances and future prospects in topical creams from medicinal plants to expedite wound healing: a review *Biotechnology \& Biotechnological Equipment* **36** 82–94

[10] Kang M S, Kwon M, Lee S H, Kim W-H, Lee G W, Jo H J, Kim B, Yang S Y, Kim K S and Han D-W 2022 3D Printing of Skin Equivalents with Hair Follicle Structures and Epidermal-Papillary-Dermal Layers Using Gelatin/Hyaluronic Acid Hydrogels. *Chem Asian J* **17** e202200620

[11] Tan S H, Ngo Z H, Sci D B, Leavesley D and Liang K 2022 Recent Advances in the Design of Three-Dimensional and Bioprinted Scaffolds for Full-Thickness Wound Healing. *Tissue Eng Part B Rev* **28** 160–81

[12] Bi H, Feng T, Li B and Han Y 2020 In Vitro and In Vivo Comparison Study of Electrospun PLA and PLA/PVA/SA Fiber Membranes for Wound Healing. *Polymers (Basel)* **12**

[13] Senthil R, Kavukcu S B and Vedakumari W S 2023 Cellulose based biopolymer nanoscaffold: A possible biomedical applications *International Journal of Biological Macromolecules* **246** 125656

[14] Liu S, Qin S, He M, Zhou D, Qin Q and Wang H 2020 Current applications of poly(lactic acid) composites in tissue engineering and drug delivery *Compos B Eng* **199** 108238

[15] Ilhan E, Ulag S, Sahin A, Ekren N, Kilic O, Oktar F N and Gunduz O 2020 Production of 3D-Printed Tympanic Membrane Scaffolds as a Tissue Engineering Application *Lecture Notes in Computer Science (including subseries Lecture Notes in Artificial Intelligence and Lecture Notes in Bioinformatics)*

[16] Choi W S, Kim J H, Ahn C B, Lee J H, Kim Y J, Son K H and Lee J W 2021 Development of a Multi-Layer Skin Substitute Using Human Hair Keratinic Extract-Based Hybrid 3D Printing. *Polymers (Basel)* **13**

[17] Platania V, Douglas T E L, Zubko M K, Ward D, Pietryga K and Chatzinikolaidou M 2021 Phloroglucinol-enhanced whey protein isolate hydrogels with antimicrobial activity for tissue engineering *Materials Science and Engineering C* **129**

[18] Guo L, Niu X, Chen X, Lu F, Gao J and Chang Q 2022 3D direct writing egg white hydrogel promotes diabetic chronic wound healing via self-relied bioactive property *Biomaterials* **282** 121406

[19] Liu Y, Hu Q, Dong W, Liu S, Zhang H and Gu Y 2022 Alginate/Gelatin-Based Hydrogel with Soy Protein/Peptide Powder for 3D Printing Tissue-Engineering Scaffolds to Promote Angiogenesis. *Macromol Biosci* **22** e2100413

[20] Domínguez-Robles J, Cuartas-Gómez E, Dynes S, Utomo E, Anjani Q K, Detamornrat U, Donnelly R F, Moreno-Castellanos N and Larrañeta E 2023 Poly(caprolactone)/lignin-based 3D-printed dressings loaded with a novel combination of bioactive agents for wound-healing applications *Sustainable Materials and Technologies* **35** e00581

[21] Garraud O, Hozzein W N and Badr G 2017 Wound healing: Time to look for intelligent, "natural" immunological approaches? *BMC Immunol* **18**

[22] Swarnalatha G and Mor S 2019 Different approaches to improve thermostability of whey proteins: a review *Int. J. Curr. Microbiol. App. Sci* **8** 1679–88

[23] Behrouz S, Saadat S, Memarzia A, Sarir H, Folkerts G and Boskabady M H 2022 The Antioxidant, Anti-Inflammatory and Immunomodulatory Effects of Camel Milk. *Front Immunol* **13** 855342

[24] Tut T A, Cesur S, Ilhan E, Sahin A, Yildirim O S and Gunduz O 2022 Gentamicin-loaded polyvinyl alcohol/whey protein isolate/hydroxyapatite 3D composite scaffolds with drug delivery capability for bone tissue engineering applications *Eur Polym J* **179** 111580

[25] Ebaid H, Salem A, Sayed A and Metwalli A 2011 Whey protein enhances normal inflammatory responses during cutaneous wound healing in diabetic rats. *Lipids Health Dis* **10** 235

[26] Badr G, Badr B M, Mahmoud M H, Mohany M, Rabah D M and Garraud O 2012 Treatment of diabetic mice with undenatured whey protein accelerates the wound healing process by enhancing the expression of MIP-1α, MIP-2, KC, CX3CL1 and TGF-β in wounded tissue *BMC Immunol* **13**

[27] Cakmak H Y, Ege H, Yilmaz S, Agturk G, Yontem F D, Enguven G, Sarmis A, Cakmak Z, Gunduz O and Ege Z R 2023 3D printed Styrax Liquidus (Liquidambar orientalis Miller)-loaded poly (L-lactic acid)/chitosan based wound dressing material: Fabrication, characterization, and biocompatibility results *Int J Biol Macromol* **248**

[28] Ilhan E, Ulag S, Sahin A, Yilmaz B K, Ekren N, Kilic O, Sengor M, Kalaskar D M, Oktar F N and Gunduz O 2020 Fabrication of tissue-engineered tympanic membrane patches using 3D-Printing technology *J Mech Behav Biomed Mater* **114** 104219

[29] Tasci M E, Dede B, Tabak E, Gur A, Sulutas R B, Cesur S, Ilhan E, Lin C C, Paik P, Ficai D, Ficai A and Gunduz O 2021 Production, optimization and characterization of polylactic acid microparticles using electrospray with porous structure *Applied Sciences (Switzerland)*

[30] Gbassi G, Yolou F, Sarr S, Atheba P, Amin C and Ake M 2012 Whey proteins analysis in aqueous medium and in artificial gastric and intestinal fluids *Int J Biol Chem Sci*

[31] Khan A, Wang C, Sun X, Killpartrick A and Guo M 2019 Preparation and characterization of whey protein isolate–dim nanoparticles *Int J Mol Sci*

[32] Ritger P L and Peppas N A 1987 A simple equation for description of solute release II. Fickian and anomalous release from swellable devices *Journal of Controlled Release* **5** 37–42

[33] Badawy M M and Allam N M 2021 Impact of Adding Protein Supplementation to Exercise Training on Lean Body Mass and Muscle Strength in Burn Patients. *J Burn Care Res* **42** 968–74

[34] Yi H C, Ibrahim Z, Abu Zaid Z, Mat Daud Z 'Azuan, Md Yusop N B, Omar J, Mohd Abas M N, Abdul Rahman Z and Jamhuri N 2020 Impact of Enhanced Recovery after Surgery with Preoperative Whey Protein-Infused Carbohydrate Loading and Postoperative Early Oral Feeding among Surgical Gynecologic Cancer Patients: An Open-Labelled Randomized Controlled Trial. *Nutrients* **12**

[35] Belokrylov G A, OYa P, Molchanova I V, Sorochinskaya E I and Anokhina V V 1992 Peptides and their constituent amino acids influence the immune response and phagocytosis in different ways. *Int J Immunopharmacol* **14** 1285–92

[36] Karageorgiou V and Kaplan D 2005 Porosity of 3D biomaterial scaffolds and osteogenesis *Biomaterials*

[37] Zhou X, Zhou G, Junka R, Chang N, Anwar A, Wang H and Yu X 2021 Fabrication of polylactic acid (PLA)-based porous scaffold through the combination of traditional bio-fabrication and 3D printing technology for bone regeneration *Colloids Surf B Biointerfaces* **197** 111420

[38] Martin V, Ribeiro I A, Alves M M, Gonçalves L, Claudio R A, Grenho L, Fernandes M H, Gomes P, Santos C F and Bettencourt A F 2019 Engineering a multifunctional 3D-printed PLA-collagen-minocycline-nanoHydroxyapatite scaffold with combined antimicrobial and osteogenic effects for bone regeneration *Materials Science and Engineering: C* **101** 15–26

[39] Zhou G, Chang W, Zhou X, Chen Y, Dai F, Anwar A and Yu X 2020 Nanofibrous Nerve Conduits with Nerve Growth Factors and Bone Marrow Stromal Cells Pre-Cultured in Bioreactors for Peripheral Nerve Regeneration *ACS Appl Mater Interfaces* **12** 16168–77

[40] Ulrich R D 1978 P. J. Flory *Macromolecular Science* 69–98

[41] Moreira A, Lawson D, Onyekuru L, Dziemidowicz K, Angkawinitwong U, Costa P F, Radacsi N and Williams G R 2021 Protein encapsulation by electrospinning and electrospraying *Journal of Controlled Release* **329** 1172–97

[42] Dissanayake M, Kasapis S, Chaudhary V, Adhikari B, Palmer M and Meurer B 2012 Unexpected high pressure effects on the structural properties of condensed whey protein systems. *Biopolymers* **97** 963–73

[43] Berton-Carabin C C, Schröder A, Rovalino-Cordova A, Schroën K and Sagis L 2016 Protein and lipid oxidation affect the viscoelasticity of whey protein layers at the oil–water interface *European Journal of Lipid Science and Technology* **118** 1630–43

[44] Gorrasi G and Pantani R 2017 Hydrolysis and Biodegradation of Poly(lactic acid) *Advances in Polymer Science*